



Vaterite microparticle-loaded methylene blue for photodynamic activity in macrophages infected with *Leishmania braziliensis*

Vitor Luca Moura Marmo¹ · Jéssica A. R. Ambrósio¹ · Erika Peterson Gonçalves¹ · Leandro José Raniero¹ · Milton Beltrame Junior¹ · Juliana G. Pinto¹ · Juliana Ferreira-Strixino¹ · Andreza R. Simioni¹

Received: 23 January 2023 / Accepted: 19 April 2023 / Published online: 28 April 2023

© The Author(s), under exclusive licence to European Photochemistry Association, European Society for Photobiology 2023

Abstract

Calcium carbonate (CaCO₃) exhibits a variety of crystalline phases, including the anhydrous crystalline polymorphs calcite, aragonite, and vaterite. Developing porous calcium carbonate microparticles in the vaterite phase for the encapsulation of methylene blue (MB) as a photosensitizer (PS) for use in photodynamic therapy (PDT) was the goal of this investigation. Using an adsorption approach, the PS was integrated into the CaCO₃ microparticles. The vaterite microparticles were characterized by scanning electron microscopy (SEM) and steady-state techniques. The trypan blue exclusion method was used to measure the biological activity of macrophages infected with *Leishmania braziliensis* in vitro. The vaterite microparticles produced are highly porous, non-aggregated, and uniform in size. After encapsulation, the MB-loaded microparticles kept their photophysical characteristics. The carriers that were captured allowed for dye localization inside the cells. The results obtained in this study indicated that the MB-loaded vaterite microparticles show promising photodynamic activity in macrophages infected with *Leishmania braziliensis*.

Keywords Methylene blue · Vaterite · Photodynamic therapy · *Leishmania*

1 Introduction

Leishmaniasis is a neglected tropical disease brought on by *Leishmania* spp. protozoan infection. There are 14 million instances of human leishmaniasis worldwide, and 350 million people are at risk of contracting the disease [1–3].

The most common cause of cutaneous leishmaniasis in Brazil, characterized by the emergence of skin ulcers, is *Leishmania braziliensis*. Mucocutaneous leishmaniasis, a crippling form of leishmaniasis accompanied by severe face tissue loss, is brought on by the metastasis of *L. braziliensis* to the oro-nasopharyngeal cavity [4, 5].

Antimonials, pentamidine, and amphotericin B, which are toxic and need monitoring of the patient and occasionally hospitalization during treatment, are still used in traditional medicine [6].

All the antileishmanial medications now on the market have certain drawbacks or side effects. The parasite has become resistant to costly chemotherapy medicines. Most developing nations' clinical misuse of drugs has been a significant factor in the spread of leishmaniasis resistance [7].

Photodynamic therapy (PDT) is a potential alternative treatment. Thus, a search for other options is essential [8, 9]. Reactive oxidant species (ROS), such as excited states, free radicals, and strong oxidants, are produced by the electronic stimulation of a photosensitive molecule (photosensitizer, PS), such as methylene blue (MB) [10].

One of the promising fields for level for better control of infectious diseases that have been steadily expanding is nanomedicine, which keeps up optimism for more accurate diagnostic tools and more effective drug delivery for a range of contagious disorders [11, 12]. Therefore, the association of PDT with novel therapeutic nano-medicine approaches is of particular significance [13, 14].

So far, various nanoparticulate systems, such as liposomes, nanoemulsions, polymeric nanoparticles, and inorganic systems, have been studied for their leishmanicidal properties [15–18].

✉ Andreza R. Simioni
simioni@univap.br

¹ Research and Development Institute—IPD, Vale do Paraíba University—UNIVAP, Av. Shishima Hifumi, 2911, São José Dos Campos, SP CEP 12244-000, Brazil

Nature has large amounts of CaCO_3 , which can be found in calcite, aragonite, and vaterite, among other forms [19]. Due to their high cell biocompatibility, calcium carbonate nanocomposite has recently received much interest [20, 21].

In Ref. [22], the authors evaluated the cytotoxicity of benznidazole-loaded calcium carbonate nanoparticles on *Trypanosoma cruzi* strain Y. In Ref. [23], the authors found that the solubility of the antiparasitic drugs praziquantel with calcium carbonate increased in an acid medium. However, the cytotoxicity study did not reveal cell death in HTC116 cells.

To the best of our knowledge, there are no reports in the literature on using calcium carbonate microparticles in the vaterite phase to assess photoactivity in *Leishmania* strains applying PDT protocols.

Thus, this study aimed to evaluate the effect of photodynamic therapy on the viability of macrophages infected with *Leishmania braziliensis* using methylene blue encapsulated in calcium carbonate microparticles in the vaterite phase. The microparticulate system's physicochemical properties were also analyzed to characterize the system.

2 Experiment

2.1 Materials

Anhydrous calcium chloride (CaCl_2), anhydrous sodium carbonate (Na_2CO_3), sodium poly (styrene sulfonate) (PSS, Mw ~ 70 KDa), trypan blue, and methylene blue were purchased from Sigma–Aldrich (St. Louis). DAPI (40,6-diamidino-2-phenylindole, dihydrochloride) was purchased from Thermofisher—ProLong™. Organic solvents in the analytical grade were purchased from Synth (Brazil) and used as received.

2.2 Particle preparation

The production of vaterite CaCO_3 particles was realized by a chemical precipitation methodology using PSS as an additive [24, 25] with some modifications. To best prepare the vaterite CaCO_3 microparticles, 0.2 mol.L^{-1} of Na_2CO_3 (pH = 11.2) and 0.5 mol.L^{-1} of CaCl_2 (pH = 6.7) solutions were mechanically stirred at high speed for 15 min in an ultra-turrax setup. This reaction typically took place in the presence of a 1% polycarboxylate-type superplasticizer. The residue was vigorously stirred before being filtered off, thoroughly rinsed with clear water, and dried in the air.

0.8 g of dried vaterite CaCO_3 microparticles were soaked in 10 mL MB to load the MB. The suspension was then brought to equilibrium after 24 h of gentle stirring. The MB-loaded vaterite CaCO_3 microparticles were then collected by centrifugation, cleaned with ethanol to remove the MB that had adhered to the outside of them, and dried in a vacuum oven at 50°C to completely evaporate the solvent from the impregnated materials (Fig. 1).

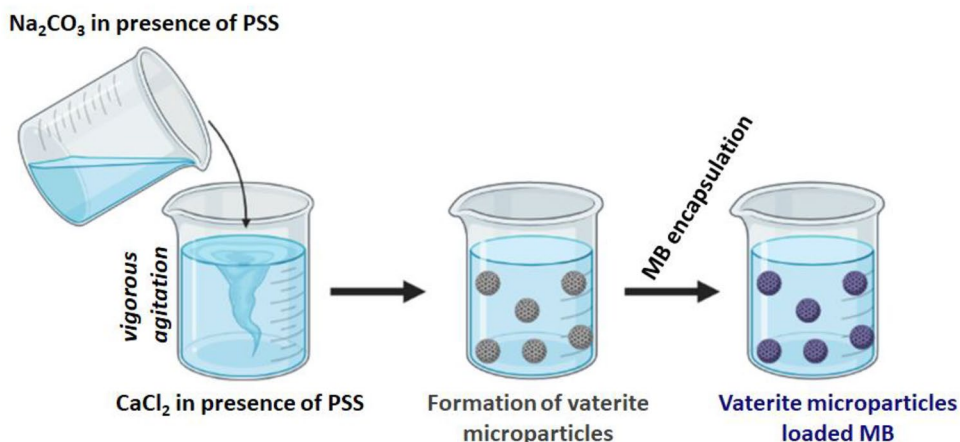
2.3 Morphology characterization

The morphologies of the samples were observed on a field emission scanning electron microscopy (SEM) using the EVO-MA10 equipment (Zeiss, Germany) (voltage 25 kV, secondary electron images). For this purpose, the samples were mounted on adhesive carbon paper, fixed with colloidal gold, and metalized with gold.

2.4 X-ray diffraction (XRD)

To better understand the crystalline phases of calcium carbonate produced, X-ray diffraction (XRD) research was carried out. The XRD spectra were captured using an XRD 6000 diffractometer from (Shimadzu Instruments, Japan)

Fig. 1 Vaterite microparticles synthesis methodology



using a Ni-filtered Cu K- α radiation source at a scan speed of 2°·min⁻¹ and a k value of 1.54439 Å.

2.5 Thermogravimetric analysis (TGA)

The thermal properties of vaterite microparticles were assessed using an STA 449 F3 Jupiter® (NETZSCH) analyzer with a heating rate of 10 °C min⁻¹ using a temperature range of 25 to 800 °C under a nitrogen atmosphere.

2.6 Differential scanning calorimetry (DSC)

DSC was carried out using an STA 449 F3 Jupiter® (NETZSCH) analyzer. The experiments used platinum crucibles in an argon atmosphere with a heating rate of 10 °C min⁻¹. The accuracy of sample mass measurement was 11.031 mg, and the accuracy in temperature measurement was 0.1 °C.

2.7 Brunauer–Emmett–Teller (BET) analysis

Using a NOVA 220e analyzer (Quantachrome, United States) and the physical gas adsorption method, the calcium carbonate particles' specific surface area and the particle pores' size distribution were measured. The specified parameters were then calculated using specialized software built into the analyzer. The adsorption isotherm was obtained after a sample of the examined material underwent preliminary degassing in a vacuum for 5 days at 35 °C. The adsorbate used was nitrogen. The specific surface areas were determined using the Brunauer–Emmett–Teller (BET) method. The Barrett–Joyner–Halenda (BJH) approach was used to define the size distribution of pores.

2.8 Fourier transform infrared (FT-IR) spectroscopy.

Fourier transform infrared spectroscopy (FTIR) was recorded on a Spectrum Spotlight 400 with Fourier Transform (FT-IR), attenuated total reflectance (ATR) technology from PerkinElmer, in the range of 450–4000 cm⁻¹ with a spectral resolution of 4 cm⁻¹ in transmittance mode with 32 scans at a controlled temperature at 20 °C.

2.9 Spectroscopic studies in the UV–visible

The data analysis allowed for the evaluation of the spectroscopic properties in both the steady state of the MB encapsulated in the vaterite microparticles and in the absence of the nanostructured system. The readings were taken with the Cary 50 spectrophotometer. These analyses allowed for the derivation of the calibration curve for MB at various concentrations and the confirmation of any changes in the

spectrum profile of the bioactive chemical when delivered to the encapsulating system.

2.9.1 Determination of incorporation efficiency (%IE)

Their weighed quantity was dissolved in an aqueous ethylenediaminetetraacetic acid solution to estimate the MB mass put into CaCO₃ containers (EDTA, 0.2 M). At 668 nm, corresponding to the maximum absorption wavelength (max) of MB, absorbance intensity was measured to represent the concentration of MB in the solution.

The incorporation efficiency (%IE) of containers was estimated according to Eq. 1:

$$\%IE = \frac{m(\text{MBloaded})}{m(\text{particles})} \times 100\% \quad (1)$$

where m (MB-loaded) is the weight of MB incorporated into vaterite microparticles, and m (particles) is the weight of vaterite microparticles.

3 In vitro experiments

3.1 Cell cultures

The macrophage line was maintained in DMEM (Dulbecco's Modified Eagle's Medium) medium supplemented with 10% Fetal Bovine Serum, 1% Penicillin/Streptomycin solution, and placed in a culture oven at 37 °C with 5% CO₂. The medium was changed every 2 days or according to cell metabolism.

The strain of *Leishmania braziliensis* (M2904) was maintained in LIT medium (Liver infusion tryptose) supplemented with 10% Fetal Bovine Serum, 2.5 mg·mL⁻¹ of hemin, 2% of sterile urine, and 1% of Penicillin/Streptomycin Solution, in a growth oven at 26 °C, and maintenance spikes were performed weekly, after determining the logarithmic growth phase of each strain.

3.1.1 Internalization of MB-loaded vaterite microparticles

The J774 macrophage line was adhered to round coverslips, at a concentration of 1×10^5 cells, in 24-well plates and kept in an oven at 37 °C and 5% ambient CO₂ overnight in DMEM medium. After this period, the infection was performed with promastigotes of *Leishmania braziliensis* in the stationary phase, in the ratio of 10:1, and incubated at 37 °C for the infection process. After that, the medium was removed and added to MB-loaded vaterite microparticles at concentrations of 0.6 and 3.0 µg·mL⁻¹ and kept at 37 °C for 1 h. The PS was removed, and the samples were washed twice with PBS (phosphate buffer saline). Coverslips were

removed from the plate and mounted with Prolong Gold antifading mounting medium with DAPI. All processing was performed in the dark, and the slides were examined in a confocal microscope LSM 700 Zeiss (λ_{exc} . DAPI: 405 nm, λ_{exc} . PS: 488 nm).

3.1.2 Analysis of cell viability of parasites by the exclusion method with trypan blue

The following groups were used for viability tests: dark control, MB-loaded vaterite microparticles at concentrations 0.6 and 3.0 $\mu\text{g}\cdot\text{mL}^{-1}$, and only vaterite microparticles at concentrations 0.6 and 3.0 $\mu\text{g}\cdot\text{mL}^{-1}$. The irradiated groups were: LED and PDT with MB-loaded vaterite microparticles at concentrations 0.6 and 3.0 $\mu\text{g}\cdot\text{mL}^{-1}$ and only vaterite microparticles at concentrations 0.6 and 3.0 $\mu\text{g}\cdot\text{mL}^{-1}$. In addition, free methylene blue was also tested at concentrations of 500, 250, 125, and 62.5 $\mu\text{g}\cdot\text{mL}^{-1}$. The irradiation process was carried out in biotable BioPDI IrradLed (660 nm, 46mW $\cdot\text{cm}^{-2}$) at a dose of 10 $\text{J}\cdot\text{cm}^{-2}$.

For this, the cells were plated and infected, as described above. After infection, the medium was removed, and PBS was added to the Control and LED groups. Next, MB-loaded vaterite microparticles and vaterite microparticles at the above concentrations and incubated them for 1 h at 37 °C. After this process, the wells were washed with PBS, and the PDT protocol was performed for the irradiated groups.

After 24 h, the medium was removed, and Trypan Blue was added at a concentration of 0.2% and incubated for 5 min. After this period, Trypan was removed, PBS was added, and images of cells were captured in 10 random fields. Live and dead cells were counted using ImageJ software. The assays were performed in quintuplicates in two separate assays.

3.1.3 Statistical analysis

All tests were performed in quintuplicates, and all data were submitted to ANOVA, followed by the Turkey test. Microsoft Excel was used to generate the charts. All data are expressed as the mean \pm standard deviation (SD) of three independent experiments. A probability p value < 0.05 was considered significant in this study.

4 Results and discussion

4.1 Morphology characterization

This study used a chemical precipitation methodology using PSS as an additive to prepare almost monodispersed vaterite microparticles from aqueous solutions in the presence of Na_2CO_3 and CaCl_2 at room temperature. This method can successfully synthesize almost monodispersed vaterite microspheres (Fig. 2).

Figures 2a, b show SEM images of the produced CaCO_3 , and SEM observations indicate that the obtained products are spherical with smooth surfaces, and their diameters are around 5 μm .

4.2 X-ray diffraction (XRD)

Calcium carbonate can be found in three stable polymorphic forms, calcite, aragonite, and vaterite, which have rhombohedral, orthorhombic, and hexagonal crystalline structures.

The qualitative analysis performed by XRD diffraction in samples synthesized by the chemical precipitation method is presented in Fig. 3.

This assay proved that the method is efficient for obtaining calcium carbonate microparticles in vaterite form. In the

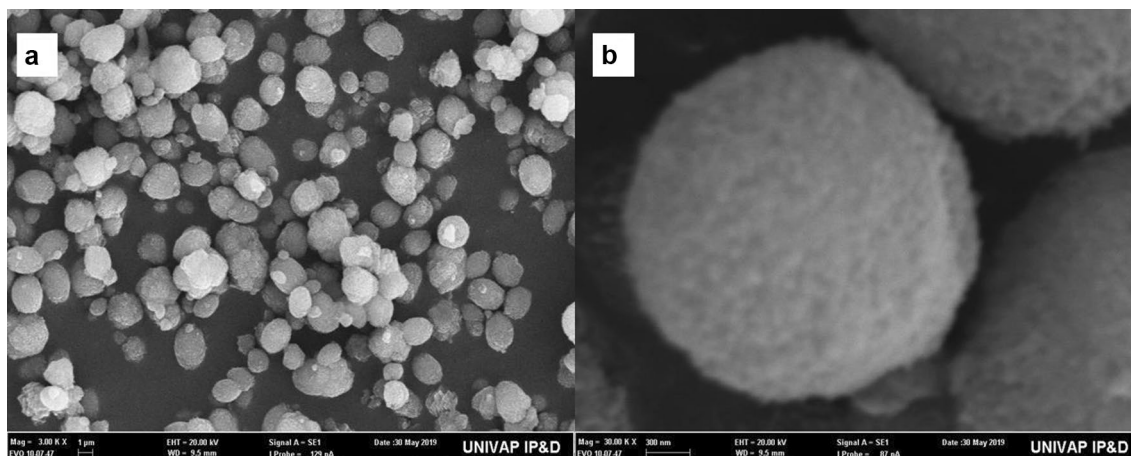
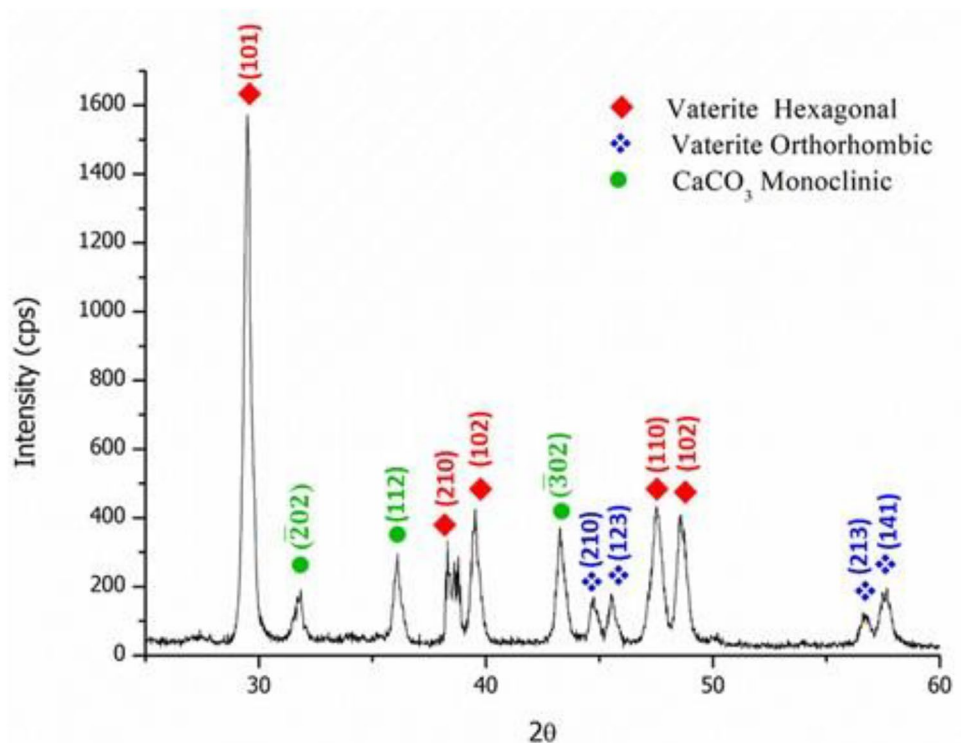


Fig. 2 Vaterite microparticles scanning electron microscopy: **a** overview of the microparticulate system formed; **b** detailing of the vaterite microparticle formed

Fig. 3 XRD data of pure and MB-loaded vaterite microparticles



result obtained, intermediate phases of unstabilized vaterite with an orthorhombic crystalline structure were observed, in addition to calcium carbonate in a metastable phase with a monoclinic crystalline form. These present phases indicate that the synthetic reaction of formation of the stable vaterite phase still needs to be completed giving rise to such intermediate compounds.

Even though the quantitative analysis by the method applied for the XRD tests is not the most appropriate, the low intensity of the peaks of the intermediate phases, when compared to the intensity of hexagonal vaterite, suggests a small amount of these intermediate phases. In addition, the stabilized hexagonal phase differs preferably in families $\{1\ 0\ 2\}$ and $\{1\ 1\ 0\}$, while the middle stages differ in different planes. However, for the application studied in this work, the presence of other polymorphic forms does not imply the impossibility of applying the material as a modified drug release system, since the morphology of the particles obtained, regardless of the crystalline habit, is presented in the spherical form as observed by SEM (Fig. 2).

4.3 Thermogravimetric analysis (TGA) and differential scanning calorimetry (DSC)

The sample's profile at high temperatures and its mass loss can be assessed using TGA and DSC analyses (Fig. 4a, b, respectively).

In the TGA analysis, the synthesized sample showed two significant peaks of mass loss, shown (Fig. 4a), the first at approximately 145 °C and the second at approximately 764 °C. Ref. [26] states that the first mass loss is attributed to removing water physically adsorbed on CaCO₃. In Ref. [27], the authors complement the analysis of the event, attributing the mass loss to the presence of additives in the CaCO₃ formulation. The second point of mass loss is described by Ref. [28] because of the CaCO₃ decomposition process.

The DSC analysis results (Fig. 4b) show a predominance of endothermic events. The only exothermic event present in the sample can be explained according to Ref. [29] by the sample crystallization process. The occurrence of the other endothermic peaks can be attributed to the transformation processes of the sample and the evaporation processes of the water present [30].

4.4 Brunauer–Emmett–Teller (BET) analysis

An essential characteristic of CaCO₃ microparticles is porosity, because it results in a high surface area, which is crucial for adsorption and desorption processes and drugs in drug delivery systems. Therefore, the Brunauer–Emmett–Teller (BET) method of adsorption/desorption of nitrogen was applied (Fig. 5) to determine this property in the particles obtained. The results showed that the effective distribution of the average diameter of the pores of CaCO₃ particles (mean diameter of 5 μm) is 58.4 ± 0.2 nm, which implies a

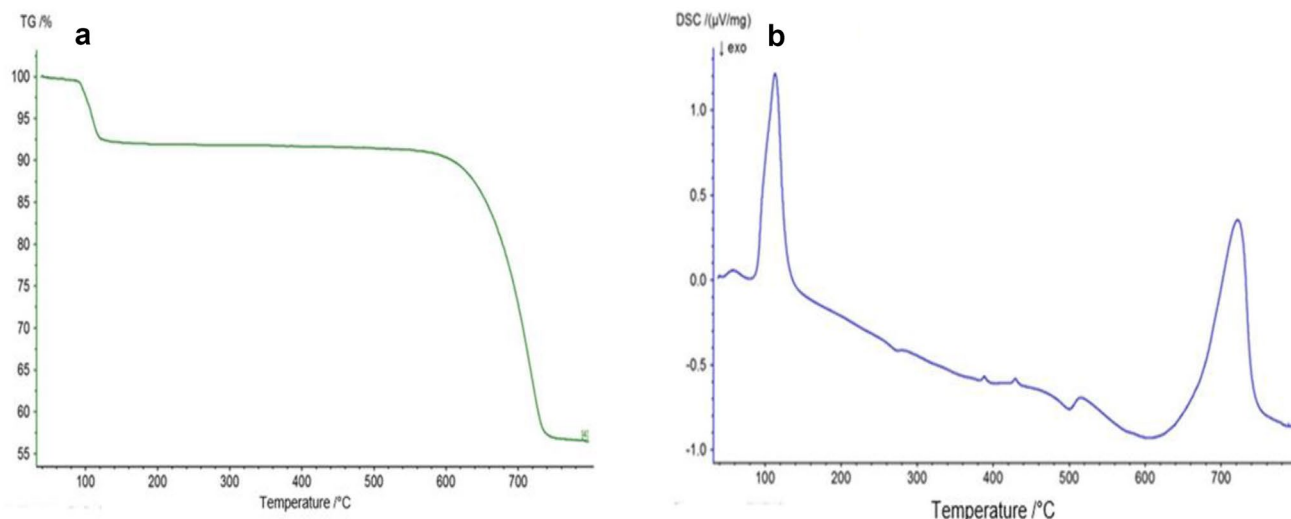
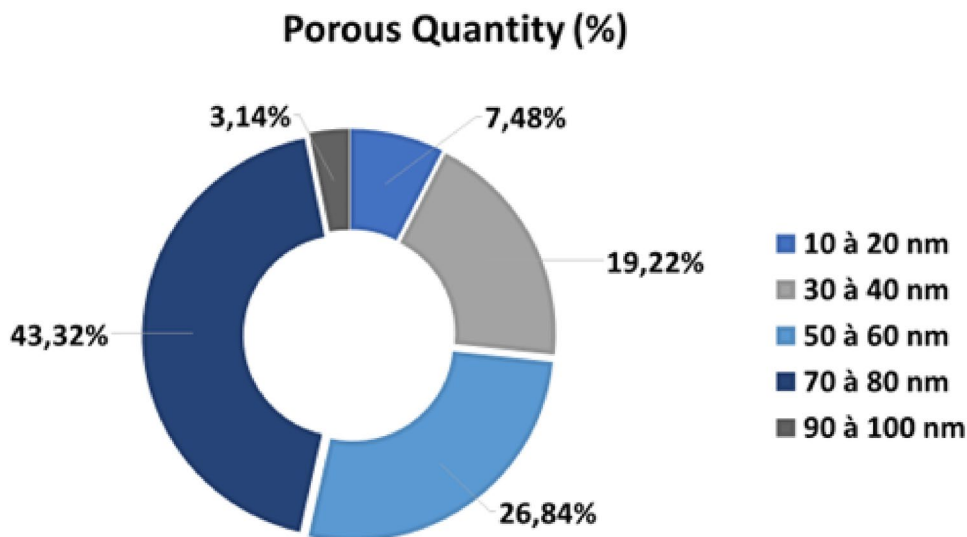


Fig. 4 **a** TGA analysis; **b** DSC analysis

Fig. 5 Size distribution of pores in the vaterite microparticles



specific surface area estimated by the BET method is $34.6 \text{ m}^2 \cdot \text{g}^{-1}$.

The wide pore size distribution may be related to the different crystalline habits identified in X-ray diffraction characterization. For example, the hexagonal phase found, according to ICDD–JCPDS no. 00-025-0127, presents a unit cell volume of $749.99 \cdot 0.106 \text{ pm}^3$ which results in lower atomic packaging factors when compared to volumes presented by phases with monoclinic structures (ICDD–JCPDS no. 00-029-0305) and orthorhombic (ICDD–JCPDS no. 01-074-1867), $239.57 \cdot 0.106 \text{ pm}^3$ and $250.41 \cdot 0.106 \text{ pm}^3$, respectively.

Vaterite-based porous crystalline calcium carbonate microspheres were created in Ref. [31]. They had a significant amount of porosity due to their large specific surface

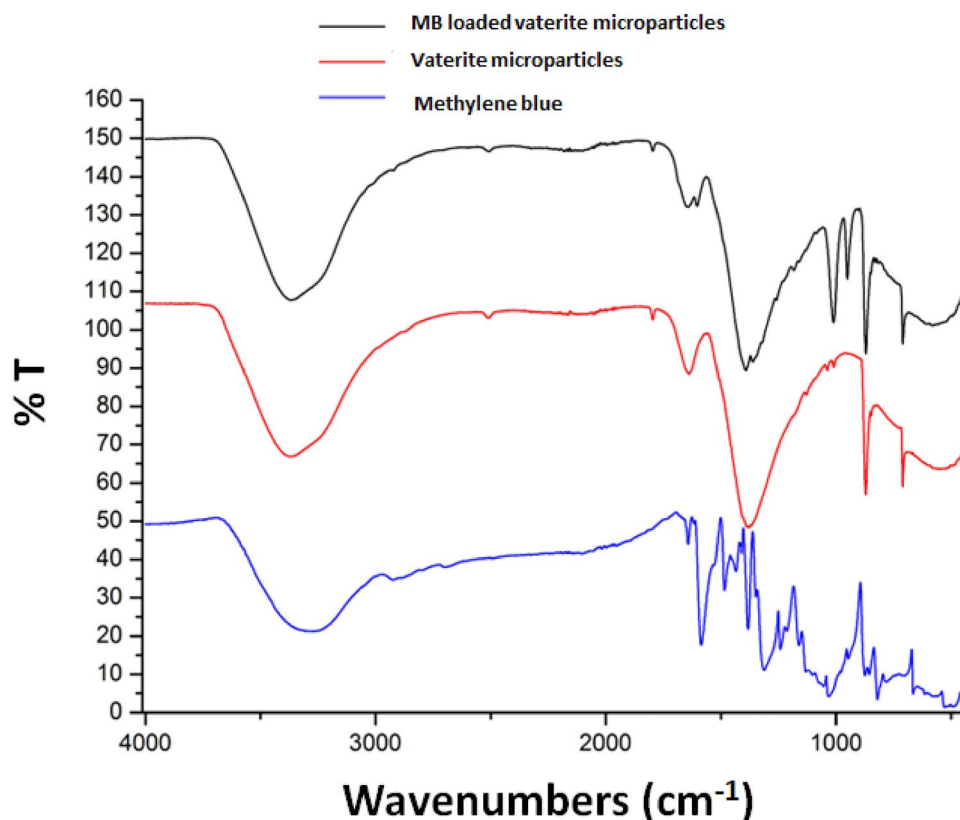
area of $16 \text{ m}^2 \cdot \text{g}^{-1}$, determined by nitrogen absorption/desorption isotherms. The prospect of employing vaterite with a high specific surface area as a drug delivery material has been suggested by recent investigations [32–34].

4.5 Fourier transform infrared (FT-IR) spectroscopy

Fourier transform-infrared (FTIR) spectroscopy was used to investigate the nature of photosensitizer incorporation into vaterite microparticles. Figure 6 shows the FTIR spectra of vaterite microparticles, free MB, and vaterite microparticles loaded with MB.

As shown in Fig. 6, the FTIR spectrum of the MB-loaded CaCO_3 microparticles shows the characteristic bands of calcium carbonate and MB absorption without the presence of

Fig. 6 FTIR spectrum



any additional vibration modes. The significant contributions in the FTIR spectrum were centered at 1088 cm^{-1} and 874 cm^{-1} , which match the bands of the calcium carbonate vaterite polymorph [35]. In the range of $1650\text{--}1595\text{ cm}^{-1}$, MB has assignments of CN (center and lateral) antisymmetric stretching + CC stretching + CH bending in plane (ring), and at 1070 cm^{-1} indicates a sulfur vibration C–S–C [36–38]. Comparing the pure methylene blue spectrum and MB-loaded CaCO_3 microparticles shows a shift in $1038\text{--}1070\text{ cm}^{-1}$ and in $1376\text{--}1390\text{ cm}^{-1}$, representing the interactions of the molecules in the microenvironment [37]. As a result, there were no discernible new bands in the spectrum, and the IR spectrum of the MB-loaded vaterite microparticles demonstrates that the CaCO_3 adsorption had a physical nature. Apart from that, the adsorption of ibuprofen into the porous CaCO_3 microparticles, Ref. [39] also explains this behavior.

4.6 Spectroscopic studies in the UV–visible

The absorbance data of vaterite microparticles encapsulated with methylene blue were compared to the data of methylene blue in free form, without the microparticles' association (Fig. 7).

Strong Q-bands in the visible area are seen in every spectrum, and peaks for MB at 658 nm occur as expected.

No change in the maximum absorption at the Q-band can be seen, indicating that the photosensitizer was mostly in a monomeric state inside the microparticles with no aggregation. A similar MB spectrum in a monomeric state was described by Fernández-Pérez & Gregorio Marbán [40]. The authors analyzed the self-aggregation of MB in water beyond the dimeric form.

As can be seen in ethanol in Fig. 8a, the chemical displayed monomeric behavior in the investigated concentration range (from 0.2 mol.L^{-1} to 4.0 mol.L^{-1}).

The least square regression demonstrated excellent correlation for the spectrophotometric approach ($r=0.99366$), and the straight-line equation was absorbance = $0.04917 \cdot [\text{MB concentration, in mol.L}^{-1}] + 0.03607$ (Fig. 8b). A satisfactory loading efficiency of $(83.8\% \pm 1,1)$ was attained. Ref. [41] developed an approach to the preparation of nanoscale particles based on CaCO_3 by coprecipitation technique for encapsulation with an anticancer drug (DOXorubicin). The authors describe that the nanoparticulate system retained more than 75% of the loaded drug within the nanocomposite. This property may ensure high selectivity of drug distribution in the context of a site-activated therapy.

Fig. 7 UV spectra MB free and encapsulated in vaterite microparticles

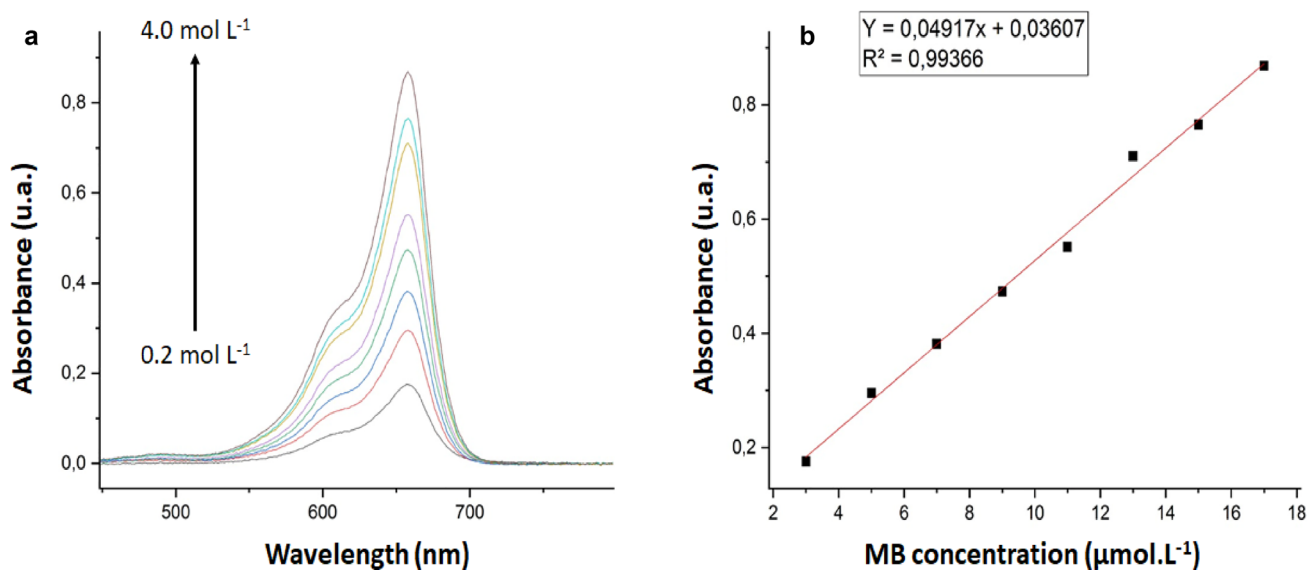
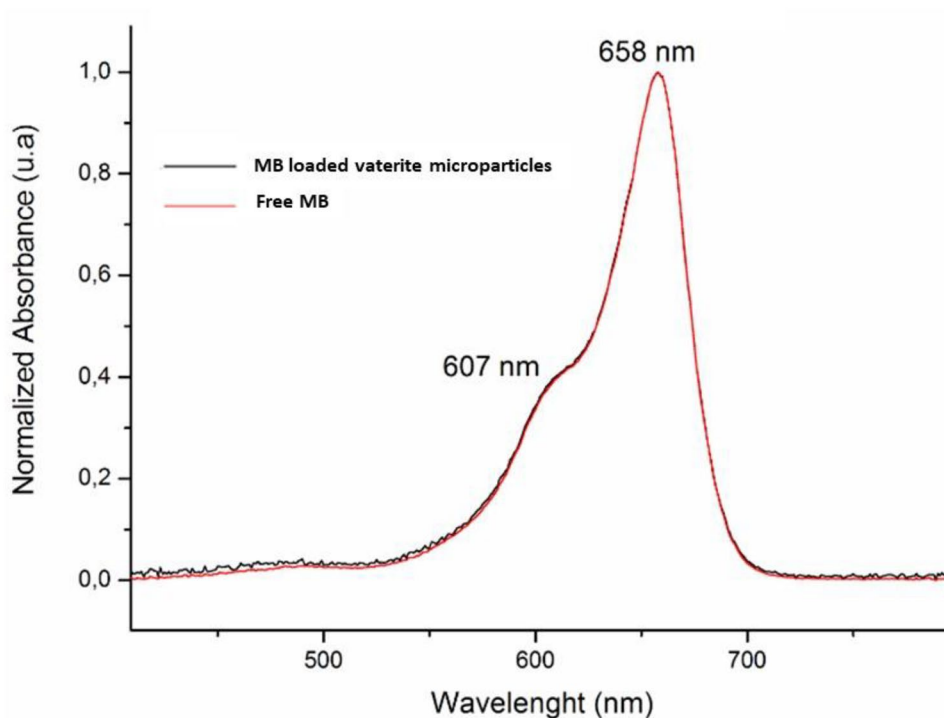


Fig. 8 MB calibration curve and linear Fit of concentration x Absorbance

4.7 Internalization of MB-loaded vaterite microparticles

Confocal fluorescence microscopy was used to evaluate the internalization of the photosensitive microparticulate system using the biological model of macrophages infected with *Leishmania braziliensis* (Fig. 9).

After 1 h of interaction, the internalization of the photosensitizer was observed in both tested concentrations, being more intense visually in the highest concentration ($3.0 \mu\text{g mL}^{-1}$). By analyzing the images, it is possible to follow that PS is in the cytoplasm of both cells, macrophages, and leishmania. It is well-known that PS's composition and chemical structure affect both its internalization and intracellular location [42].

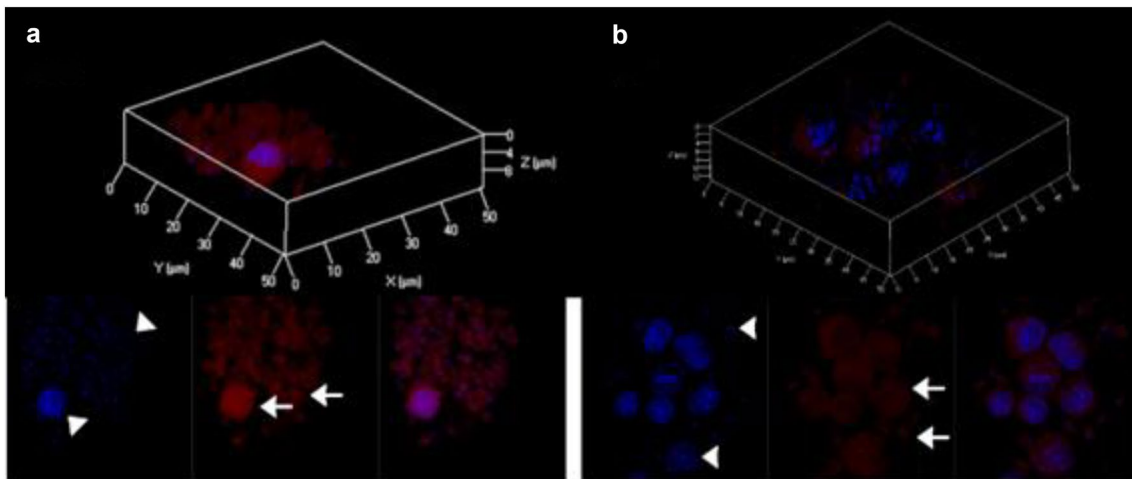


Fig. 9 Confocal fluorescence microscopy showing the photosensitizer inside the macrophages and protozoa of *Leishmania braziliensis*, in red, indicated by the arrow. The genetic material was marked with

DAPI, showing the nucleus of the cells (arrowhead). **A** The concentration of 3.0 µg.mL⁻¹, **B** Concentration of 0.6 µg.mL⁻¹

4.8 Analysis of cell viability of parasites by the exclusion method with trypan blue

Methylene Blue is a widely used dye for Photodynamic Therapy, with previously described leishmanicidal activity and the ability to internalize and affect *Leishmania* promastigotes inside the macrophage [43–46]. Data showing the interaction of free MB in pure macrophages and macrophages infected with *Leishmania* were added, indicating that MB in high concentrations is toxic in the dark for macrophages, infected or not, but at concentrations of 125 µg.mL⁻¹ and 62, 5 µg.mL⁻¹ after irradiation there was complete inactivation (Fig. 10).

After the incubation with the MB-loaded vaterite micro-particles was observed alterations in the mitochondrial activity of infected cells presented a significant reduction in the mitochondrial activity when compared with the control group ($p \leq 0.01$) (Fig. 11).

The viability test showed that although the groups that received treatment had their mitochondrial activity substantially disrupted, the viability was not impaired the same way in the groups kept in the dark. The present study also demonstrates that the encapsulation process reduces the concentration of MB necessary to reduce the viability of infected macrophages.

Fig. 10 Evaluation of the viability of free or infected macrophages with *Leishmania braziliensis* after incubation with MB at concentrations of 500, 250, 125 and 62.5 µg.mL⁻¹ ($p \leq 0.01$)

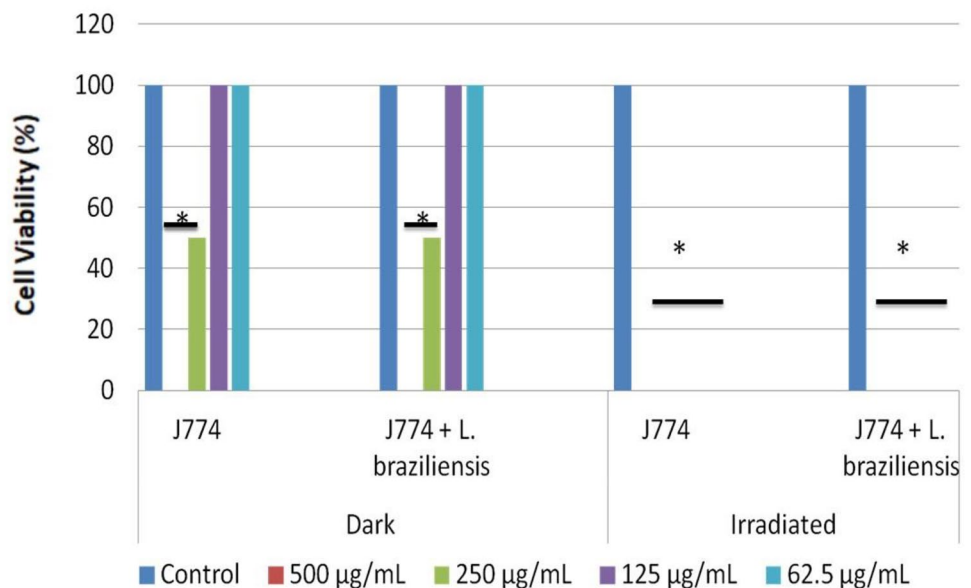
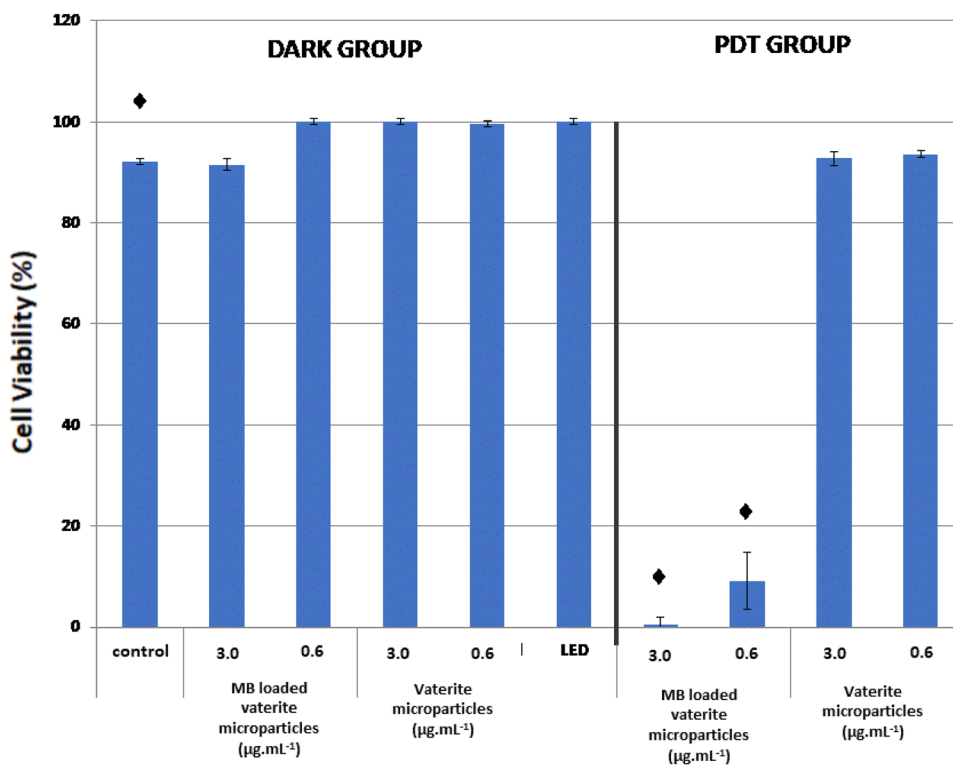


Fig. 11 Impact of different tests on the viability of macrophages infected with *Leishmania braziliensis*. A significant difference between the PDT groups with MB-loaded vaterite microparticles 3.0 and 0.6 $\mu\text{g}\cdot\text{mL}^{-1}$ and the dark control ($p \leq 0.01$)



Ref. [47] studied macrophages infected with *L. amazonensis* and *L. braziliensis* using various phthalocyanines, and they noted different response patterns of the infected macrophages. Compared to *L. braziliensis*-infected macrophages, *L. amazonensis*-infected macrophages were more responsive to treatment in the presence of zinc phthalocyanine (ZnPc), whereas *L. braziliensis*-infected macrophages were more responsive to treatment in the presence of tetraaminophthalocyanine zinc (PcZn4NH₂) [39]. In addition, the aluminum phthalocyanine tetrasulfonate (AlPcS₄) treatment used 10 $\mu\text{mol}\cdot\text{L}^{-1}$ and 10 $\text{J}\cdot\text{cm}^{-2}$ to lower viability by 90% in *L. braziliensis* while only reducing it by roughly 70% in *L. major*, demonstrated that *L. braziliensis* strains are more vulnerable to other PDT methods.

Methylene Blue is a widely used dye for Photodynamic Therapy, with previously described leishmanicidal activity and the ability to internalize and affect *Leishmania* promastigotes inside the macrophage [43, 44]. Its effect was previously demonstrated in free promastigotes of different species, such as *Leishmania major* and *Leishmania braziliensis*, in vitro, having presented the impact on the mitochondrial activity and on the viability and morphology of the parasites. Low MB toxicity was demonstrated in promastigotes after 1 h of interaction and kept in the dark. However, after irradiation with 10 J/cm^2 , the viability was significantly altered [47]. Furthermore, studies with Fourier Transform Infrared Spectroscopy (FT-IR) after PDT with MB showed that both species, *L. braziliensis*, and *L. major*, present biochemical

changes after PDT with MB, such as increased lipids and proteins [48, 49].

In Reference [44], the antiparasitic effect of PDT with MB was analyzed in macrophages infected with *Leishmania braziliensis* and treated with MB at a concentration of 12.5 $\mu\text{g}\cdot\text{mL}^{-1}$, and irradiated with 8.4 J/cm^2 (660 nm, 40 mW), observing reduced infection rate in groups treated with PDT.

These data indicate that although MB is viable for use in the inactivation of macrophages infected with PDT, the encapsulation process reduces the concentration of PS necessary to obtain macrophage inactivation. This behavior is interesting for future clinical application, aiming to treat cutaneous lesions of leishmaniasis.

5 Conclusion

Vaterite microparticles are templates for encapsulating methylene blue, a photosensitizing compound in photodynamic therapy protocols. The microparticulate system was characterized by techniques, such as XRD, BET, and SEM. As demonstrated by FTIR, MB is incorporated in vaterite microparticles by physical adsorption. Confocal fluorescence microscopy showed the photosensitizer inside the macrophages and protozoa of *Leishmania braziliensis*. The exclusion test with Trypan Blue showed that PDT with the compound MB-loaded vaterite microparticles significantly

reduced the viability of infected cells. Based on the results obtained, it is expected that vaterite microparticles encapsulated with MB can be promising adjuvant in the leishmaniasis treatment based on the application of PDT protocols, contributing to the scientific and technological development of science with a potential degree of innovation and impact on society.

Acknowledgements The authors acknowledge the financial support of the Brazilian agency FAPESP (Fundação de Amparo à Pesquisa do Estado de São Paulo) with project number 2018/18531-6.

Data availability The data supporting this study's findings are available from the corresponding author upon reasonable request.

Declarations

Conflict of interest The authors declare no potential conflict of interest in this work.

References

- Domingues, K. L. T. G., Tanoshi, C. A., Noma, I. H. Y., Carvalho, M. D. B., Aristides, S. M. A., Demarchi, I. G., Pedrosa, R. B., & Lonardon, M. V. C. (2022). Economic impact of hospitalizations due to leishmaniasis in southern Brazil. *Research Society and Development*, *11*, e39211831139–e39211831149. <https://doi.org/10.33448/rsd-v11i8.31139>
- Sharma, R., Viana, S. M., Ng, D. K. P., Kolli, B. K., Chang, K. P., & de Oliveira, C. I. (2020). Photodynamic inactivation of *Leishmania braziliensis* doubly sensitized with uroporphyrin and diamino-phthalocyanine activates effector functions of macrophages in vitro. *Scientific Reports*, *10*, 17065–17078. <https://doi.org/10.1038/s41598-020-74154-1>
- Pal, M., Ejeta, I., Girma, A., Dave, K., & Dave, P. (2022). Etiology, clinical spectrum, epidemiology, diagnosis, public health significance and control of Leishmaniasis: A comprehensive review. *Acta Scientific Microbiology*, *5*, 140–151. <https://doi.org/10.31080/ASMI.2022.05.1066>
- Tironi, F. C., Machado, G. U., Arruda, S. M., & Machado, P. R. L. (2021). Plantar ulcer as an atypical manifestation of cutaneous leishmaniasis. *Anais Brasileiros de Dermatologia*, *96*, 352–354. <https://doi.org/10.1016/j.abd.2020.06.015>
- Anversa, L., Tiburcio, M. G. S., Richini-Pereira, V. B., & Ramirez, L. E. (2018). Leishmaniose humana no Brasil: Uma revisão geral. *Revista da Associação Médica Brasileira*, *64*, 281–289. <https://doi.org/10.1590/1806-9282.64.03.281>
- Sundar, S., & Chakravarty, J. (2015). An update on pharmacotherapy for leishmaniasis. *Expert Opinion on Pharmacotherapy*, *16*, 237–252. <https://doi.org/10.1517/14656566.2015.973850>
- Wijnant, G. J., Dumetz, F., Dirckx, L., Bulte, D., Cuyper, B., Bocxlaer, K. V., & Hendrickx, S. (2022). Tackling drug resistance and other causes of treatment failure in leishmaniasis. *Frontiers in Tropical Diseases*, *3*, 1–23. <https://doi.org/10.3389/ftd.2022.837460>
- Vital-Fujii, D. G., & Baptista, M. S. (2021). Progress in the photodynamic therapy treatment of Leishmaniasis. *Brazilian Journal of Medical and Biological Research*, *54*, e11570–e11580. <https://doi.org/10.1590/1414-431X2021e11570>
- Varzandeh, M., Mohammadinejad, R., Esmailzadeh-Salestani, K., Dehshahri, A., Zarrabi, A., & Aghaei-Afshar, A. (2021). Photodynamic therapy for leishmaniasis: Recent advances and future trends. *Photodiagnosis and Photodynamic Therapy*, *36*, 102609–102615. <https://doi.org/10.1016/j.pdpdt.2021.102609>
- Correia, J. H., Rodrigues, J. A., Pimenta, S., Dong, T., & Yang, Z. (2021). Photodynamic therapy review: principles photosensitizers, applications, and future directions. *Pharmaceutics*, *13*, 1332–1347. <https://doi.org/10.3390/pharmaceutics13091332>
- Kirtane, A. R., Verma, M., Karandikar, P., Furin, J., Langer, R., & Traverso, G. (2021). Nanotechnology approaches for global infectious diseases. *Nature Nanotechnology*, *16*, 369–384. <https://doi.org/10.1038/s41565-021-00866-8>
- Tobin, E., & Brenner, S. (2021). Nanotechnology fundamentals applied to clinical infectious diseases and public health. *Open Forum Infectious Diseases*, *8*, 1–10. <https://doi.org/10.1093/ofid/ofab583>
- Goonoo, N., Huët, M. A. L., Chummun, I., Karuri, N., Badu, K., Gimié, F., Bergrath, J., Schulze, M., Müller, M., & Bhaw-Luximon, A. (2022). Nanomedicine-based strategies to improve treatment of cutaneous leishmaniasis. *Royal Society Open Science*, *9*, 220058–220085. <https://doi.org/10.1098/rsos.220058>
- Hernández, I. P., Montanari, J., Valdivieso, W., Morilla, M. J., Romero, E. L., & Escobar, P. (2012). In vitro phototoxicity of ultradeformable liposomes containing chloroaluminum phthalocyanine against new world *Leishmania* species. *Photochemistry and Photobiology B: Biology*, *117*, 157–163. <https://doi.org/10.1016/j.jphotobiol.2012.09.018>
- Mukherjee, S., Pradhan, S., Ghosh, S., Sundar, S., Das, S., Mukherjee, B., & Roy, S. (2020). Short-course treatment with imipramine entrapped in squalene liposomes results in sterile cure of experimental visceral leishmaniasis induced by antimony resistant leishmania donovani with increased efficacy. *Frontiers in Cellular and Infection Microbiology*, *10*, 1–10. <https://doi.org/10.3389/fcimb.2020.595415>
- Pinto, S. M. L., Muehlmann, L. A., Ojeda, L. L. M., Arias, A. M. V., Cordero, M. V. R., Santos, M. F. M. A., Azevedo, R. B., & Rivero, P. E. (2021). Nanoemulsions with chloroaluminium phthalocyanine and paromomycin for combined photodynamic and antibiotic therapy for cutaneous leishmaniasis. *Infection and Chemotherapy*, *53*, 342–354. <https://doi.org/10.3947/ic.2021.0010>
- Saqib, M., Bhatti, A. S. A., Ahmad, N. M., Ahmed, N., Shahnaz, G., Lebaz, N., & Elaissari, A. (2020). Amphotericin B loaded polymeric nanoparticles for treatment of *Leishmania* infections. *Nanomaterials*, *10*, 1152–1167. <https://doi.org/10.3390/nano10061152>
- Khatami, M., Alijani, H. Q., Mousazadeh, F., Hashemi, N., Mahmoudeh, Z., Darjani, S., Bamorovat, M., Keyhani, A., Abdollahpour-Alitappeh, M., & Borhani, F. (2020). Calcium carbonate nanowires: Greener biosynthesis and their leishmanicidal activity. *RSC Advances*, *10*, 38063–38068. <https://doi.org/10.1039/D0RA04503A>
- Sekkal, W., & Zaoui, A. (2013). Nanoscale analysis of the morphology and surface stability of calcium carbonate polymorphs. *Scientific Reports*, *3*, 1587–1597. <https://doi.org/10.1038/srep01587>
- Shi, R. J., Lang, J. Q., Wang, T., Zhou, N., & Ma, M. G. (2022). Fabrication properties, and biomedical applications of calcium-containing cellulose-based composites. *Frontiers in Bioengineering and Biotechnology*, *10*, 937266–937275. <https://doi.org/10.3389/fbioe.2022.937266>
- Popova, V., Poletaeva, Y., Pyshnaya, I., Pyshnyi, D., & Dmitrienko, E. (2021). Designing pH-dependent systems based on nanoscale calcium carbonate for the delivery of an antitumor drug. *Nanomaterials*, *11*, 2794–2309. <https://doi.org/10.3390/nano11112794>
- Tessarolo, L. D., de Menezes, R. R. P. B., Mello, C. P., Lima, D. B., Magalhães, E. P., Bezerra, E. M., Sales, F. A. M., Barroso Neto, I. L., Oliveira, M. F., dos Santos, R. P., Albuquerque, E.

- L., Freire, V. N., & Martins, A. M. (2018). Nanoencapsulation of benzimidazole in calcium carbonate increases its selectivity to *Trypanosoma cruzi*. *Parasitology*, *145*, 1191–1198. <https://doi.org/10.1017/S0031182018000197>
23. Borrego-Sánchez, A., Sánchez-Espejo, R., Albertini, B., Passerini, N., Cerezo, P., Viseras, C., & Sainz-Díaz, C. I. (2019). Ground calcium carbonate as a low cost and biosafety excipient for solubility and dissolution improvement of praziquantel. *Pharmaceutics*, *11*, 533–545. <https://doi.org/10.3390/pharmaceutics11100533>
 24. Jiang, J., Wu, Y., Chen, C., Wang, X., Zhao, H., Xu, S., Yang, C. C., & Xiao, B. (2018). A novel route to prepare the metastable vaterite phase of CaCO₃ from CaCl₂ ethanol solution and Na₂CO₃ aqueous solution. *Advanced Powder Technology*, *29*, 2416–2422. <https://doi.org/10.1016/j.apt.2018.06.020>
 25. Souza, E. F., Ambrósio, J. A. R., Pinto, B. C. S., Beltrame, M., Sakane, K. K., Pinto, J. G., Ferreira-Strixino, J., Gonçalves, E. P., & Simioni, A. R. (2020). Vaterite submicron particles designed for photodynamic therapy in cells. *Photodiagnosis and Photodynamic Therapy*, *31*, 101913–101919. <https://doi.org/10.1016/j.pdpdt.2020.101913>
 26. Zhang, Y., Qiao, L., Yan, H., Zizak, I., Zaslansky, P., Li, Y., Qi, L., & Ma, Y. (2020). Vaterite microdisc mesocrystals exposing the (001) facet formed via transformation from proto-vaterite amorphous calcium carbonate. *Crystal Growth & Design*, *20*, 3482–3492. <https://doi.org/10.1021/acs.cgd.0c00259>
 27. Dou, J., Zhao, F., Fan, W., Chen, Z., & Guo, X. (2020). Preparation of non-spherical vaterite CaCO₃ particles by flash nano precipitation technique for targeted and extended drug delivery. *Journal of Drug Delivery Science and Technology*, *57*(2020), 101768–110775. <https://doi.org/10.1016/j.jddst.2020.101768>
 28. Remya, K. P., Kim, S., & Kim, M. (2022). Surfactant-free hydrothermal fabrication of vaterite CaCO₃ with hexagonal bipyramidal morphologies using seawater. *Powder Technology*, *410*, 117865–117873. <https://doi.org/10.1016/j.powtec.2022.117865>
 29. Jensen, A. C. S., Birkedal, H., & Bertinetti, L. (2019). Co-incorporation of alkali metal ions during amorphous calcium carbonate precipitation and their stabilizing effect. *Physical Chemistry Chemical Physics*, *21*, 13230–13233. <https://doi.org/10.1039/C9CP02437A>
 30. Ashokan, A., Rajendran, V., Kumar, T. S., & Jayaraman, G. (2021). Process optimization for the rapid conversion of calcite into hydroxyapatite microspheres for chromatographic applications. *Ceramics International*, *47*, 18575–18583. <https://doi.org/10.1038/s41598-022-16579-4>
 31. Beuquier, T., Calvignac, B., Delcroix, G. J. R., Tran, M. K., Kodjikian, S., Delorme, N., Bardeau, J. F., Gibaud, A., & Boury, F. (2011). Synthesis of hollow vaterite CaCO₃ microspheres in supercritical carbon dioxide medium. *Journal of Materials Chemistry*, *26*, 9757–9761. <https://doi.org/10.1039/C1JM10770D>
 32. Huang, Y., Cao, L., Parakhonskiy, B. V., & Skirtach, A. G. (2022). Hard, soft, and hard-and-soft drug delivery carriers based on CaCO₃ and alginate biomaterials: synthesis properties, pharmaceutical applications. *Pharmaceutics*, *14*, 909–951. <https://doi.org/10.3390/pharmaceutics14050909>
 33. Sun, R., Willhammar, T., Grape, E. S., Strømme, M., & Cheung, O. (2019). Mesoscale transformation of amorphous calcium carbonate to porous Vaterite microparticles with morphology control. *Crystal Growth & Design*, *19*, 5075–5087. <https://doi.org/10.1021/acs.cgd.9b00438>
 34. Sun, R., Zhang, P., Bajnóczi, E. G., Neagu, A., Tai, C. W., Persson, I., Strømme, M., & Cheung, O. (2018). Amorphous calcium carbonate constructed from nanoparticle aggregates with unprecedented surface area and mesoporosity. *ACS Applied Materials & Interfaces*, *10*, 21556–21564. <https://doi.org/10.1021/acsami.8b03939>
 35. Abeykoon, K. G. M. D., Dunuweera, S. P., Liyanage, D. N. D., & Rajapakse, R. M. G. (2020). Removal of fluoride from aqueous solution by porous Vaterite calcium carbonate nanoparticles. *Materials Research Express*, *7*, 035009–0350020. <https://doi.org/10.1088/2053-1591/ab7692>
 36. Aoki, P. H. B., Volpati, D., Caetano, W., & Constantino, C. J. L. (2010). Study of the interaction between cardiolipin bilayers and methylene blue in polymer-based Layer-by-Layer and Langmuir films applied as membrane mimetic systems. *Vibrational Spectroscopy*, *54*, 93–102. <https://doi.org/10.1016/j.vibspec.2010.03.013>
 37. Ovchinnikov, O. V., Evtukhova, A. V., Kondratenko, T. S., Smirnov, M. S., Khokhlov, V. Y., & Erina, O. V. (2016). Manifestation of intermolecular interactions in FTIR spectra of methylene blue molecules. *Vibrational Spectroscopy*, *86*, 181–186. <https://doi.org/10.1016/j.vibspec.2016.06.016>
 38. Samyn, L. M., Babu, R. S., Devendiran, M., & Barros, A. L. F. (2021). One-step electropolymerization of methylene blue films on highly flexible carbon fiber electrode as supercapacitors. *Micro and Nano Systems Letters*, *9*, 1–10. <https://doi.org/10.1186/s40486-021-00130-7>
 39. Wang, C., He, C., Tong, Z., Liu, X., Ren, B., & Zeng, F. (2006). Combination of adsorption by porous CaCO₃ microparticles and encapsulation by polyelectrolyte multilayer films for sustained drug delivery. *International Journal of Pharmaceutics*, *308*, 160–167. <https://doi.org/10.1016/j.ijpharm.2005.11.004>
 40. Fernández-Pérez, A., & Marbán, C. (2020). Visible light spectroscopic analysis of methylene blue in water: What comes after dimer? *ACS Omega*, *5*, 29801–29815. <https://doi.org/10.1021/acsomega.0c03830>
 41. Lakkakula, J. R., Kurapati, R., Tynga, I., Abrahamse, H., Raichur, A. M., & Krause, R. W. M. (2016). The mechanism of catalase loading into porous vaterite CaCO₃ crystals by co-synthesis. *RSC Advances*, *6*, 104537–104548. <https://doi.org/10.1039/C7CP07836F>
 42. Pinto, J. G., Marcolino, L. M. C., & Ferreira-Strixino, J. (2021). Photodynamic activity of Photogem® in *Leishmania* promastigotes and infected macrophages. *Future Microbiology*, *16*, 95–106. <https://doi.org/10.2217/fmb-2020-0019>
 43. Muel, J., Jörg, S., & Baggiolini, M. (1984). Intracellular parasite killing induced by electron carriers. II. Correlation between parasite killing and the induction of oxidative events in macrophages. *Molecular and Biochemical Parasitology*, *13*, 97–110.
 44. de Oliveira, S., Trahamane, E. J. O., Monteiro, J., Santos, G. P., Crujeira, P., Oliveira, C., Neto, M. B., & Pinheiro, A. (2017). Leishmanicidal effect of antiparasitic photodynamic therapy-ApPDT on infected macrophages. *Lasers in Medical Science*, *32*, 1959–1964. <https://doi.org/10.1007/s10103-017-2292-9>
 45. Pinto, J. G., Martins, J. F. S., Pereira, A. H. C., Mittmann, J., Raniero, L. J., & Ferreira-Strixino, J. (2017). Evaluation of methylene blue as photosensitizer in promastigotes of *Leishmania* major and *Leishmania braziliensis*. *Photodiagnosis and Photodynamic Therapy*, *18*, 325–330. <https://doi.org/10.1016/j.pdpdt.2017.04.009>
 46. Aureliano, D. P., Lindoso, J. A. L., Soares, S. R. C., Takakura, C. F. H., Pereira, T. M., & Ribeiro, M. S. (2018). Cell death mechanisms in *Leishmania amazonensis* triggered by methylene blue-mediated antiparasitic photodynamic therapy. *Photodiagnosis and Photodynamic Therapy*, *23*, 1–8.
 47. Silva, E. P. D. O., Mittmann, J., Ferreira, V. T. P., Cardoso, M. A. G., & Beltrame, M. (2015). Photodynamic effects of zinc phthalocyanines on intracellular amastigotes of *Leishmania amazonensis* and *Leishmania braziliensis*. *Lasers in Medical Science*, *30*, 347–354. <https://doi.org/10.1007/s10103-014-1665-6>
 48. Fagundes, J., Sakane, K. K., Bhattacharjee, T., Pinto, J. G., Ferreira, I., Raniero, L. J., & Ferreira-Strixino, J. (2019). Evaluation

- of photodynamic therapy with methylene blue, by the fourier transform infrared spectroscopy (FT-IR) in Leishmania major-in vitro. *Spectrochimica Acta Part A: Molecular and Biomolecular Spectroscopy*, 2017, 229–235. <https://doi.org/10.1016/j.saa.2018.09.031>
49. Sakane, K. K., Bhattacharjee, T., Fagundes, J., Marcolino, L. M. M., Ferreira, I., Pinto, J. G., & Ferreira-Strixino, J. (2021). Biochemical changes in *Leishmania braziliensis* after photodynamic therapy with methylene blue assessed by the Fourier transform infrared spectroscopy. *Lasers in Medical Science*, 36, 821–827. <https://doi.org/10.1007/s10103-020-03110-2>

Springer Nature or its licensor (e.g. a society or other partner) holds exclusive rights to this article under a publishing agreement with the author(s) or other rightsholder(s); author self-archiving of the accepted manuscript version of this article is solely governed by the terms of such publishing agreement and applicable law.